

Searching for stars ejected from the Galactic Centre in *DESI*

Sill Verberne¹*, Sergey E. Koposov^{2,3}, Elena Maria Rossi¹, and Zephyr Penoyre¹

¹ Leiden Observatory, Leiden University, P.O. Box 9513, 2300 RA Leiden, the Netherlands

² Institute for Astronomy, University of Edinburgh, Royal Observatory, Blackford Hill, Edinburgh EH9 3HJ, UK

³ Institute of Astronomy, University of Cambridge, Madingley Road, Cambridge CB3 0HA, UK

Received XXX / Accepted YYY

ABSTRACT

Dynamical interactions between stars and the super massive black hole Sgr A* at the Galactic Centre (GC) may eject stars into the Galactic halo. While recent fast ejections by Sgr A* have been identified in the form of hypervelocity stars (hundreds to thousands km/s), it is also expected that the stellar halo contains slower stars, ejected over the last few billion years. In this study, we use the first data release of *DESI* to search for these slower GC ejecta, which are expected to stand out from the stellar halo population for their combined high metallicity ($[\text{Fe}/\text{H}] \gtrsim 0$) and small values of their vertical angular momentum (L_z), whose distribution should peak at zero. Our search does not yield a detection, but allows us to place an upper limit on the ejection rate of stars from the GC of $\sim 2.8 \times 10^{-3} \text{ yr}^{-1}$ over the past ~ 5 Gyr, which is ejection model independent. This implies that our result can be used to put constraints on different ejection models, including that invoking mergers of Sgr A* with other massive black holes in the last few billion years.

Key words. The Galaxy – Galaxy: halo – Galaxy: center – Galaxy: stellar content – Galaxy: kinematics and dynamics

1. Introduction

The stellar halo is a highly complex environment made up of substructures containing information on the assembly history of the Galaxy. In particular, with the advent of *Gaia* (Gaia Collaboration et al. 2016) a wealth of knowledge has been gathered on the individual components of the halo (for a recent review, see Deason & Belokurov 2024). We now understand that the halo is perhaps entirely made up of the debris of past merger events. This means that the halo provides a means of studying the remains of high-redshift dwarf galaxies in great detail given the relative proximity of halo stars.

In our understanding of the halo, we rarely consider the effect of the Galactic Centre (GC) and in particular the super massive black hole Sagittarius A* (Sgr A*). However, there is reason to think that this might not be entirely justified. In recent decades, it has become clear that Sgr A* ejects stars on unbound trajectories travelling through the halo by the Hills mechanism (Hills 1988; Yu & Tremaine 2003; Brown et al. 2005; Brown 2015; Koposov et al. 2020). Moreover, a significant fraction of these ejected stars is expected to remain bound to the Galaxy (e.g. Bromley et al. 2006; Rossi et al. 2014). This introduces a population of stars with the chemical properties of the GC that populate the halo (Brown et al. 2007). Stars ejected from the GC are often referred to as hypervelocity stars (HVSs), but here we will refer to them as GC ejecta, since we focus on the stars still bound to the Galaxy, rather than the unbound population.

GC ejecta provide interesting science cases, since they are windows into the complex GC environment in parts of the sky that are easier to study, while unlocking wavelength ranges for observations that are inaccessible to sources at the GC. In addition, their trajectories can be used as traces of the Galactic potential (e.g. Contigiani et al. 2019; Gallo et al. 2022). However,

their application has been limited so far, because only a single unambiguous star ejected from the GC is known (Koposov et al. 2020), alongside a handful of promising candidates (Brown et al. 2005, 2014, 2018). A big factor in the difficulty to accurately identify HVSs is that many of these candidates tend to be distant, which makes their past trajectories uncertain. The rate and properties of GC ejecta are therefore also still uncertain (Zhang et al. 2013; Brown et al. 2014; Marchetti et al. 2022; Evans et al. 2022a,b). The best constraints on the rate so far have been published in Verberne et al. (2024, 2025), who find an upper limit of 10^{-5} yr^{-1} for stars more massive than $1 M_\odot$ and an enhanced ejection rate over the past 10 Myr of about 10^{-4} yr^{-1} .

Additionally, past mergers of Sgr A* with intermediate or supermassive black holes would have boosted the rate of stars ejected from the GC by orders of magnitude (e.g. Yu & Tremaine 2003; Evans et al. 2023). For these reasons, it is unknown how large the halo population of GC ejecta is.

In this work, we aim to constrain the population of GC ejecta that has built up in the stellar halo over the lifetime of the Galaxy. We expect that two characteristic features can be used to identify these stars:

1. Metal rich, since they originated in the GC (e.g. Schultheis et al. 2019; Schödel et al. 2020), and
2. Initial orbital angular momentum is zero, since these stars are ejected radially from the GC.

No other stellar halo populations are known with metallicities similar to the GC, making the metallicity a crucial factor in the identification of this population of stars. We used the recently released Dark Energy Survey Instrument (*DESI*; DESI Collaboration et al. 2016) Data Release 1 (DR1; DESI Collaboration et al. 2025) in combination with *Gaia* DR3 (Gaia Collaboration et al. 2023) to calculate the angular momenta for individual stars. We used the distributions of angu-

* verberne@strw.leidenuniv.nl

lar momenta and $[\text{Fe}/\text{H}]$ to search for a statistical overdensity of low-angular momentum, high-metallicity stars.

The structure of this work is as follows: we start by discussing the origin of GC ejecta and our simulations in Section 2, followed by a description of the observations we use in Section 3. In Section 4, we discuss our method for identifying a possible population of GC ejecta, before we present our results in Section 5. In Section 6, we discuss our assumptions and put our results in perspective. Finally, in Section 7, we summarise our work.

2. Galactic Centre ejecta

In this section, we start by discussing a mechanism through which stars can be ejected from the GC and end up in the stellar halo, before we describe how we implement this in our simulations. We explain the specific ejection mechanism used in our simulations below, but we argue that our results are in fact ejection model independent (see Section 6.1).

2.1. Hills mechanism

The Hills mechanism (Hills 1988) acts on a stellar binary that approaches a massive black hole within the tidal radius, where the tidal force of the black hole separates the stellar binary, ejecting one star and capturing its companion (for review, see Brown 2015). The ejected stars can gain enough energy to become unbound to the Galactic potential. For a contact binary progenitor, for instance, the ejected star can be ejected at up to about 3500 km s^{-1} (Rossi et al. 2014). However, a significant fraction of ejected stars will remain bound to the Galaxy, travelling on highly eccentric orbits. Although the fraction of stars that remain bound to the Galaxy is a function of the binary progenitor population properties, in particular the mass ratio and semi-major axis distributions, a population of stars ejected from the GC will accumulate in the stellar halo. For a star ejected from the GC on a bound orbit in a perfect axisymmetric potential we expect L_Z to be conserved and equal to 0, while L_X and L_Y will oscillate due to the gravity of the disc.

The number of stars in this population is highly uncertain mainly because the ejection rate is only constrained to an order of magnitude and the progenitor binary properties are poorly constrained. Most literature estimates of the ejection rate are between 10^{-3} and 10^{-5} yr^{-1} (Hills 1988; Yu & Tremaine 2003; Zhang et al. 2013; Brown et al. 2014; Marchetti et al. 2022; Evans et al. 2022b; Verberne et al. 2024) and are based on recent (past $\sim 100 \text{ Myr}$) ejections. Verberne et al. (2025) extended this with a lower limit of the ejection rate over about a billion years of $\sim 10^{-5} \text{ yr}^{-1}$.

2.2. Simulations

To predict the physical and observational footprint of the population of stars ejected from the GC, we perform a suite of simulations.

Our starting point is the simulations presented in Verberne et al. (2025, section 3 and 4), which we refer to for a detailed description. To summarize here, we sample from a progenitor binary population defined by the star formation history, initial mass function, log-period distribution, and mass ratio distribution. In Verberne et al. (2025) two progenitor populations are described: a young population with an average ejection rate over the past $\sim 10 \text{ Myr}$ of approximately 10^{-4} yr^{-1}

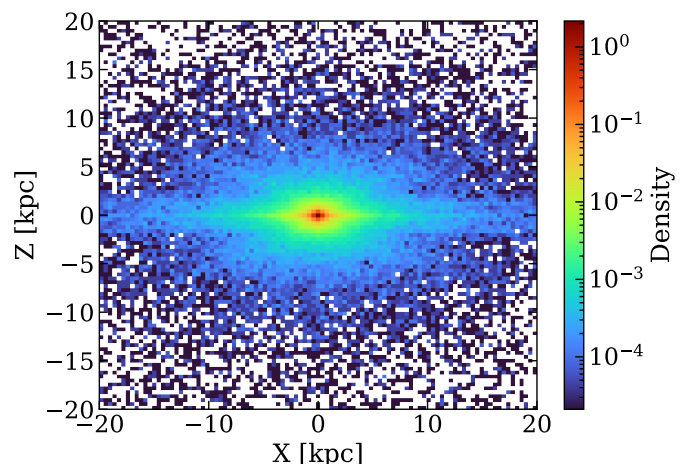


Fig. 1: Galactic Cartesian X–Z distribution of the GC ejecta propagated in the McMillan (2017) potential over 5 Gyr.

and an old population with an ejection rate of at least $\sim 10^{-5} \text{ yr}^{-1}$ over potentially billion-year timescales. We focus here on the old population, but we note that past bursts of star formation near Sgr A* might have boosted the ejection rate, similar to what seems to have happened recently with the formation of the clockwise disc.

We randomly select one of the stars in the progenitor binary to be ejected regardless of its mass, as appropriate for incoming centre of mass parabolic trajectories, (which is realistic; Sari et al. 2009; Kobayashi et al. 2012). We assume that stars are isotropically ejected from the GC and evolve their orbits using Agama (Vasiliev 2019a) in the McMillan (2017) Galactic potential until the ‘present time’. We consider stars ejected over the past 5 Gyr to allow significant accumulation of ejected stars in the halo. We evaluate our choice of potential by comparing it with a non-axisymmetric potential in Section 6.2.

To obtain observational parameters for our simulated stars, in particular the star brightness in different photometric bands, we utilise MIST isochrones (Dotter 2016; Choi et al. 2016). This allows us to forward model the population of ejected stars observable by *DESI* (DESI Collaboration et al. 2025). Furthermore, we use PyGaia¹ to obtain estimated uncertainties on the measured parallax of stars in our simulations.

2.3. Results from simulations

Now that we have presented our simulations, we will discuss some of the key results they provide, which will help guide our search for GC ejecta in *DESI* DR1.

We only analyse ejected stars with an apocentre above 0.1 kpc for computational reasons and because we are mainly interested in the ejected stars that reach the stellar halo. Firstly, we examine the distribution of GC ejecta in Galactocentric Cartesian coordinates in Fig. 1. Although stars are isotropically ejected from the GC, we can see that gravitational focussing by the disc causes many ejected stars to end up in or near the stellar disc, which is in the $Z = 0$ plane (see also Kenyon et al. 2018). Of particular interest compared to stellar halo populations is the radial density profile, which we show in Fig. 2. In our definition, the fraction of stars n is calculated from the density $\rho(r)$ as $n = \int 4\pi r^2 \rho(r) dr$. We perform a least-squares fit using a power

¹ <https://github.com/agabrown/PyGaia>

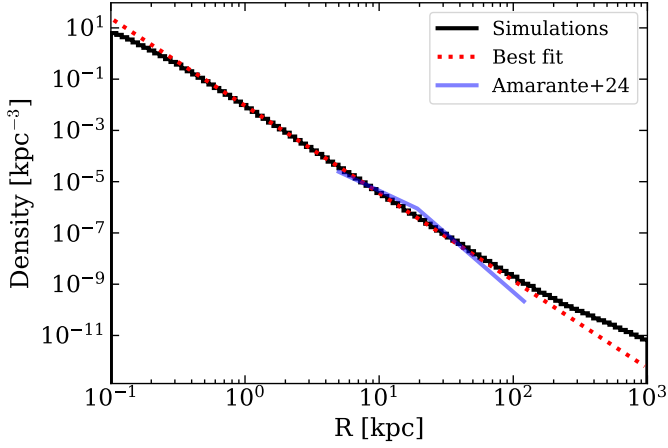


Fig. 2: Radial density profile of the population of stars ejected from the GC in the McMillan (2017) potential. The red line shows the best fit power-law in the range [1, 100] kpc, $\rho \propto r^{-3.41 \pm 0.01}$. For reference we show the halo profile found in Amarante et al. (2024), which we scale to our data at the solar circle.

law of the form $\rho(r) = \rho_0 r^{-\alpha}$ to the range [1, 100] kpc. We find a power-law slope of $\alpha = 3.41 \pm 0.01$, which is significantly steeper compared to the stellar halo within ~ 20 kpc, but tends to be less steep compared to measurements of the stellar halo outside ~ 20 kpc (e.g. Bell et al. 2008; Xue et al. 2015; Amarante et al. 2024; Yu et al. 2024). Moreover, at distances above about 100 kpc there is an overdensity compared to the simple power-law slope caused by unbound stars.

Another key characteristic of GC ejecta is their angular momentum distribution. To calculate the angular momentum of a star, we need the proper motion, radial velocity, and distance. We combine the proper motion from *Gaia* DR3 (Gaia Collaboration et al. 2023), the RVSpecFit (RVS) radial velocity from the *DESI* Milky Way Survey (MWS) value-added catalogue (Koposov et al. 2024), and the distance from the *DESI* spectrophotometric distance value-added catalogue (Li et al. 2025). However, before we can present the expected distribution of L_Z in *DESI*, we first need to discuss the observational selection function. The one of the MWS bright survey in *DESI* is described in Cooper et al. (2023) and Koposov et al. (2025). We approximate it as follows:

- $16 < r < 19$,
- $\text{Dec} > -15$ deg,
- $|b| > 40$ deg,
- completeness = 20%,
- $(g - r < 0.7) \mid (g - r > 0.7 \wedge \varpi < 3\sigma_\varpi + 0.3)$,

where ϖ and σ_ϖ are the parallax and corresponding uncertainty respectively. We know that the observed spread in the distribution of L_Z for GC ejecta in an axisymmetric potential will be dominated by observational uncertainty in the distance to individual stars, since $L_Z = 0$ intrinsically. To account for this, we randomly sample from the distribution of distance/uncertainty for sources in the Li et al. (2025) value-added distance catalogue, for each simulated star. We convolve the true distances to the simulated stars with these uncertainties, only considering sources with distance/uncertainty > 5 , since these will be the sources we analyse in Section 3. From our procedure, we obtain the expected observed angular momentum distribution for GC

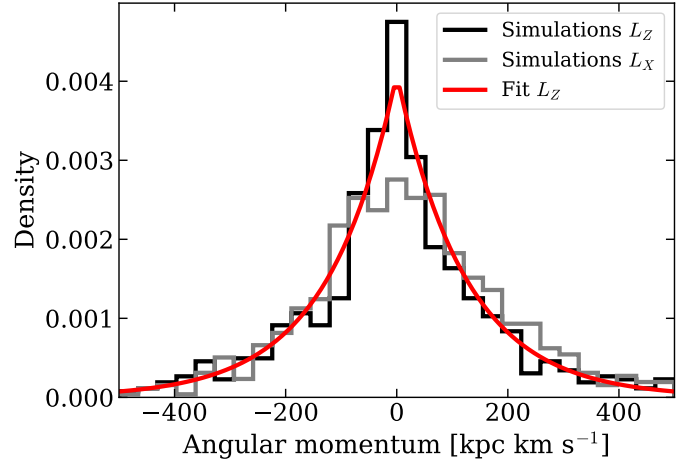


Fig. 3: Measured distribution of L_Z/L_X for GC ejecta in the simulations. Since the true L_Z of ejected stars is 0, the observed spread is due to distance uncertainties. We provide a fit to the data in red. In grey we also plot the measured L_X distribution.

ejecta in *DESI*, shown in Fig. 3. While the distribution in L_Z is exclusively set by the distance uncertainty, the spread in L_X is a combination of the intrinsic L_X distribution and the distance uncertainty. We perform an unbinned fit with a Laplace distribution of the form

$$f(x \mid \mu, b) = \frac{1}{2b} \exp\left(-\frac{|x - \mu|}{b}\right) \quad (1)$$

to the L_Z distribution shown in Fig. 3, where we fix the offset $\mu = 0$. This provides us with the scale parameter for which we find the 50th percentile value $b = 1.2 \times 10^2$ kpc km s $^{-1}$ (narrower than other populations, see Section 4). We will use this distribution and shape as the characteristic shape of GC ejecta in the *DESI* data, and evaluate the (in)dependence of the assumed ejection model on our results in Section 6.1.

Given our simulations and the selection function of *DESI*, we can also compute the number of GC ejecta in the *DESI* MWS bright catalogue given an ejection rate. For GC ejecta from the old population we referenced above, we expect $\sim 0.18 * \frac{\eta}{10^{-5} \text{ yr}^{-1}}$ GC ejecta stars in *DESI*, with η the average ejection rate over the past 5 Gyr. Furthermore, we expect that recent ejections from the young population will contribute $\sim 0.27 * \frac{\eta}{10^{-4} \text{ yr}^{-1}}$ GC ejecta for an ejection rate of 10^{-4} yr^{-1} during the past 10 Myr to *DESI*. These estimates are likely somewhat pessimistic, since the bright programme includes some sources outside the selection function estimate that we use. Moreover, past mergers between Sgr A* and massive black holes could have additionally ejected large numbers of stars from the GC through the "slingshot mechanism" that are not accounted for in our simulations, as we mentioned in our introduction.

3. Observations

In the previous section, we have already discussed the observational selection function and forward modelling of *DESI*. Here we will describe the specific observational data from *DESI* used in this study.

We rely on data from *DESI* DR1 and in particular on the MWS catalogue (Cooper et al. 2023). The MWS catalogue contains spectra and properties derived from ~ 5 M stars. Especially of interest to this work are the value added catalogues

that have simultaneously been published. Here we use the radial velocities and [Fe/H] abundance measurements from the RVSpecFit (RVS) pipeline (Koposov 2019; Cooper et al. 2023) in combination with the distances from the spectrophotometric MWS SpecDis catalogue (Li et al. 2025). For the [Fe/H] measurements, we use the calibration described in Koposov et al. (2025), which makes the measurements accurate to ~ 0.1 dex. Note that this recalibration is very important for our results, since high metallicity giants in *DESI* show a systematic offset towards too high [Fe/H] in RVS².

To ensure that we only use reliable measurements, we apply the following data quality cuts in *DESI*:

- SUCCESS = True (RVS flag),
- RVS_WARN = 0,
- FEH_ERR < 0.2,
- RR_SPECTYPE = STAR,
- DIST/DISTERR > 5.

Finally, we use the crossmatch of *DESI* and *Gaia* from the MWS value-added catalogue, to obtain proper motion measurements.

4. Different populations in the L_Z –[Fe/H] plane

Now that we have discussed our simulations and the observational data set, we will describe how we analyse the data from *DESI* to find this population of stars ejected from the GC. We also discuss stellar populations that might be misclassified as GC ejecta because of possible overlap in parameter space.

In the Introduction, we identified two characteristic properties that we expect for stars ejected from the GC over the past several billion years: we expect them to be metal rich and travel on initially radial trajectories. We discussed in Section 2.2 how these stars oscillate in L_X and L_Y , while L_Z remains constant at 0. We therefore attempt to find a statistical overdensity of high-metallicity stars with an angular momentum distribution centred at $L_Z = 0$. Furthermore, we know the shape of the angular momentum distribution in L_Z , since we expect this shape to be dominated by the observational uncertainties in the distances to individual stars, as discussed in Section 2.2.

In order to identify an overdensity in [Fe/H]– L_Z space, it is important to understand what other populations of stars overlap in this parameter space with GC ejecta. To gain intuition for this parameter space, we show metallicity against L_Z for all stars in our observational dataset (see Section 3) in Fig. 4. At low metallicity ($-2 < [\text{Fe}/\text{H}] < -1$) and centred at $L_Z = 0$ we can see the population known as *Gaia*-Sausage/Enceladus (GSE; Belokurov et al. 2018; Helmi et al. 2018; Haywood et al. 2018). GSE dominates the stellar halo in the solar neighbourhood and consists of metal-poor stars (mean [Fe/H] ~ -1.2 ; Feuillet et al. 2021) on highly eccentric orbits (for review, see Deason & Belokurov 2024). This population of stars is believed to be the remains of the most recent major merger of the Milky Way, which occurred ~ 10 Gyr ago. The L_Z distribution of GSE peaks roughly at $L_Z = 0$, the same as the GC ejecta. However, unlike our expectation for GC ejecta, GSE does have a measurable width in L_Z space by *DESI*.

Metallicity is the other important differentiator: the metal-rich boundary of the GSE is typically found at around

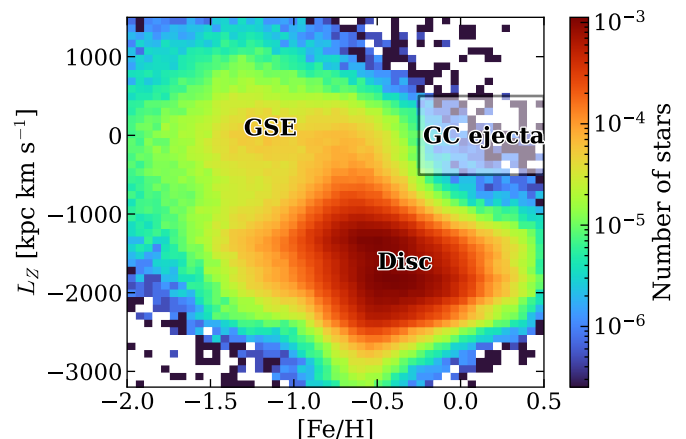


Fig. 4: Histogram of [Fe/H] against L_Z for stars in the selection in *DESI* DR1 described in Section 3. We highlight areas occupied by different galactic components and GC ejecta.

[Fe/H] ~ -0.6 (e.g. Myeong et al. 2019; Hasselquist et al. 2021; Horta et al. 2023), much lower in metallicity compared to typical stars expected from the GC (Do et al. 2015; Feldmeier-Krause et al. 2017; Schödel et al. 2020; Feldmeier-Krause et al. 2025). However, it is not excluded that there is a more metal-rich compact GSE remnant (e.g. Hasselquist et al. 2021). Finally, uncertainties in the measured [Fe/H] might lead to the misclassification of a GSE star.

The other population of stars that can end up in the high-metallicity, low-angular-momentum part of parameter space comes from the (thick) disc. In Fig. 4, we can see that most stars reside at large negative L_Z , but a tail towards low angular momenta extends from this population. This tail is possibly related to the recently discovered population of relatively metal-rich ([Fe/H] > -0.7) stars on highly eccentric orbits known as ‘Splash’ (Belokurov et al. 2020). These stars have little to no angular momentum and their relatively high metallicity means that they might overlap significantly with GC ejecta. A suggested interpretation of the Splash is that these stars were part of the protodisc of the Galaxy and were kicked out during the merger event that created GSE.

For detailed information on these and other halo populations, we refer to recent reviews (e.g. Rix & Bovy 2013; Bland-Hawthorn & Gerhard 2016; Deason & Belokurov 2024; Hunt & Vasiliev 2025).

4.1. Fitting the L_Z –[Fe/H] plane

Now that we have a better understanding of the background stellar populations at high metallicity and low angular momentum, we will describe our model.

We perform all our fits in L_Z space in bins of metallicity. Furthermore, we separately treat dwarfs and giants, which we separate at $\log g = 4$ as determined in the *DESI* MWS catalogue from RVS. We focus on the region $|L_Z| < 500$ kpc km s^{−1}, since the population extending from large negative L_Z can be described by a linear slope in this region. We will refer to this population as the Splash. To describe the GSE, we use a Gaussian centred at $L_Z = 0$ and determine the width in the L_Z space by performing an unbinned fit of this Gaussian and a linear slope to the distribution of L_Z with $|L_Z| < 500$ kpc km s^{−1} and $-1.7 < [\text{Fe}/\text{H}] < -1.3$. We find a standard deviation of ~ 170 kpc km s^{−1} for giants and ~ 410 kpc km s^{−1} for dwarfs and use these values to fix the width

² Without the metallicity recalibration from Koposov et al. (2025), we find an overdensity of high-metallicity giants centred at $L_Z = 0$. The recalibration shifts these stars to lower metallicities, consistent with the *Gaia*-Sausage/Enceladus halo population.

in L_Z of GSE for our fits in metallicity bins. We leave the slope of the Splash population as a free parameter.

Our probability density function to describe the distribution of stars in L_Z within the range $[-L_{Z, \max}, L_{Z, \max}]$ per bin of metallicity is then

$$f(L_Z) = p_{\text{GSE}} \frac{1}{\sqrt{2\pi}\sigma^2} \exp\left(-\frac{L_Z^2}{2\sigma^2}\right) \frac{1}{Z_{\text{norm, GSE}}} + p_{\text{ej}} \frac{1}{2b} \exp\left(-\frac{|L_Z|}{b}\right) \frac{1}{Z_{\text{norm, ej}}} + (1 - p_{\text{GSE}} - p_{\text{ej}}) \left(\frac{1}{2L_{Z, \max}} + aL_Z \right), \quad (2)$$

where p_{GSE} and p_{ej} are the fractions of stars belonging to in the GSE and the GC ejecta respectively, σ the width of the GSE in L_Z , $Z_{\text{norm, GSE}}$ and $Z_{\text{norm, ej}}$ the integrals of the normal and Laplace distributions respectively over the range $[-L_{Z, \max}, L_{Z, \max}]$, b the scale parameter of the GC ejecta, and a the slope of the linear Splash population.

For bins in metallicity, we perform unbinned fits to the probability density function for $L_{Z, \max} = 500 \text{ kpc km s}^{-1}$ using a Markov Chain Monte Carlo (MCMC) approach. We use 100 walkers, with 500 burn-in steps and 1000 additional steps to explore the posterior and calculate percentile confidence intervals. The free parameters in this fit are p_{GSE} , p_{ej} , and a . We use uniform priors on p_{GSE} and p_{ej} between 0 and 1, and for a we use a uniform prior for $|a| \leq 1/(2L_{Z, \max})$, so that the posterior is positive for $|L_Z| < L_{Z, \max}$. Finally, we require that $1 - p_{\text{GSE}} - p_{\text{ej}} \geq 0$, such that our probability density function integrates to 1.

5. Results

Now that we have discussed our model and the data, we will look at our results.

In Fig. 5, we show the fraction and number of stars that belong to the Splash, GSE, and GC ejecta populations, as a function of metallicity. The fraction of GC ejecta is always consistent with 0 if we consider that $p_{\text{ej}} \geq 0$ and the fact that the posteriors are highly non-Gaussian given this truncation. In fact, the posterior on p_{ej} usually peaks at $p_{\text{ej}} = 0$. For dwarfs we can see that at low metallicity the Splash and GSE contribute about equally to the stellar population, while for giants the Splash always dominates. Note that these numbers are not necessarily representative for the 'true' fractions in the halo, since we do not correct for observational selection effects nor is our model optimised for detecting populations other than GC ejecta.

So far, we have not made any selections on angular momentum other than in L_Z . However, for GC ejecta, we expect that L_X is also centred and concentrated around $L_X = 0$. To improve our statistics, we perform an additional fit selecting only $L_X < 300 \text{ kpc km s}^{-1}$ to constrain the contribution from the GC ejecta population to the metallicity bin $-0.25 < [\text{Fe}/\text{H}] < 0.5$. We chose this metallicity bin to encompass all GC ejecta. For both dwarfs and giants we again find a fraction of GC ejecta consistent with 0. The 95% upper limit on the number of GC ejecta within this metallicity bin is about 38 dwarfs and 13 giants, for a total of about 51 stars. However, not all GC ejecta will be in our observational sample. The 95% upper limit on the number of GC ejecta with $16 < r < 19$ and $|b| > 40 \text{ deg}$ can be written as

$$N_{\text{GC, ej}}^{95}(16 < r < 19 \wedge |b| > 40 \text{ deg}) = \frac{p_{\text{ej}}^{95} N_{[\text{Fe}/\text{H}]}}{C_{\text{spec}} C_{\text{colour}} C_{\text{Dec}} C_L}, \quad (3)$$

with p_{ej}^{95} the 95% upper limit on the fraction of GC ejecta, $N_{[\text{Fe}/\text{H}]}$ the number of stars in the metallicity bin, and C_{spec} , C_{colour} , C_{Dec} , and C_L the completenesses on the spectroscopy, colour selection, Dec range, and angular momentum respectively. The spectroscopic completeness of *DESI* DR1 is 20% as mentioned before and we calculate from our simulations that the product of the other completeness factors is about 60%. The total number of GC ejected stars with $16 < r < 19$ at $|b| > 40$ can therefore be no higher than $51/(0.2 \cdot 0.6) \simeq 4.3 \times 10^2$ at the 95% confidence limit, assuming that the ejection mechanism is isotropic.

The upper limit for the number of GC ejecta in *DESI* implies constraints on the ejection rate of stars from the GC over a timescale of billions of years, since GC ejecta will have accumulated in the halo for billions of years. Since we expect $\sim 0.18 \cdot \frac{\eta}{10^{-5} \text{ yr}^{-1}}$ GC ejecta in *DESI* for an ejection rate η (see, Sec. 2.3), the average ejection rate over this timescale has to be at most $\sim 2.8 \times 10^{-3} \text{ yr}^{-1}$.

6. Discussion

In this section, we provide context for our results, review some of our assumptions, and discuss future prospects. Since our simulations (excluding orbit integrations) are directly taken from the work of Verberne et al. (2025), we refer to that paper for a discussion of the ejection model and the progenitor binary population assumptions.

In this work, we investigated whether we could identify an overdensity of high-metallicity stars at low angular momenta in the Galactic halo using data from *DESI* DR1. Such a population could point to Hills mechanism disruptions of binary stars near Sgr A* or past mergers of Sgr A* with intermediate mass or massive black holes. Our analysis yields a non-detection that we use to constrain the GC ejection rate over a timescale of $\sim 5 \text{ Gyr}$, a novelty with respect to previous constraints obtained with unbound stars which were therefore limited to the shorter timescales of their fly times ($\sim 100 \text{ Myr}$). Specifically, we conclude that the average ejection rate over the past $\sim 5 \text{ Gyr}$ cannot exceed $\sim 2.8 \times 10^{-3} \text{ yr}^{-1}$. This rate is in line with previous estimates and constraints for the Hills mechanism, which tend to span the range $10^{-3} - 10^{-5} \text{ yr}^{-1}$ (Hills 1988; Yu & Tremaine 2003; Bromley et al. 2012; Zhang et al. 2013; Brown et al. 2014; Evans et al. 2022a,b; Marchetti et al. 2022; Verberne et al. 2024, 2025).

6.1. Testing the ejection model dependence

Here we evaluate the dependence of our results on the specific ejection model assumed. A previous study showed that the velocity distribution of stars ejected from the GC is determined by the potential rather than the ejection velocity spectrum for stars travelling on bound orbits (Rossi et al. 2014). We verify that this holds for our simulations by using different ejection velocity distributions. We find that the width of the zero angular momentum population and the number of expected GC ejecta in *DESI* are not significantly affected, which means that our results hold for any population of stars ejected isotropically from the GC and are thus ejection model independent.

6.2. Testing the (non-)axisymmetric potential dependence

So far, we have used the axisymmetric McMillan (2017) potential for our orbit integration. The effect is that the intrinsic L_Z distribution is a delta function at $L_Z = 0$ and the spread in the

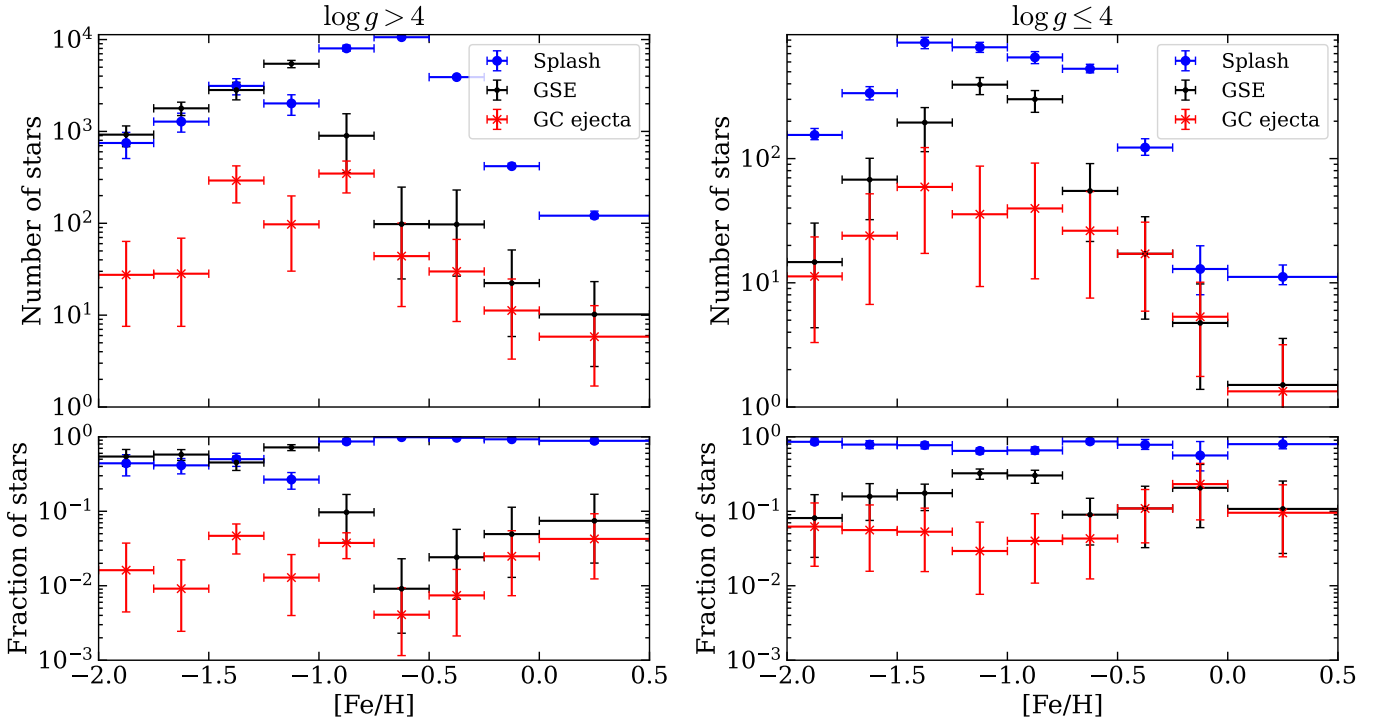


Fig. 5: Relative contributions of Splash, GSE, and GC ejecta for stars with $|L_z| < 500 \text{ kpc km s}^{-1}$ as a function of metallicity. The rows show the number of stars and fraction in each population respectively, while the columns show dwarfs and giants. The horizontal error bars correspond to the bin size in $[\text{Fe}/\text{H}]$, while the vertical error bars are from the 16th and 84th percentiles of the posterior.

observed L_z distribution is exclusively caused by observational uncertainties. However, the potential of the Galaxy contains non-axisymmetric components that will impart L_z onto GC ejecta. To investigate this effect, we make use of the potential defined in Hunter et al. (2024, excluding Sgr A*), which contains the nuclear star cluster, nuclear stellar disk, bar, thin and thick stellar disks, gas disks, dark halo, and spiral arms. Both the bar and spiral arms are non-axisymmetric and are rotating in this potential. We follow the same procedure we used for the McMillan (2017) potential and integrate the orbits using Agama. The result of the non-axisymmetric components is that the L_z distribution becomes wider, with a scale parameter of $\sim 1.5 \times 10^2 \text{ kpc km s}^{-1}$, compared to $\sim 1.2 \times 10^2 \text{ kpc km s}^{-1}$ for the McMillan (2017) potential. We also evaluate if the increased width in L_z affects our conclusions, by reanalysing the *DESI* data using our model (equation 2) with this increased width of the GC ejecta population. We find that the increased width of the L_z distribution does not significantly impact the ratios of stars we assign to the Splash, GSE, or GC ejecta populations. Our rate and number constraints for GC ejecta increase by about 15% if we assume the Hunter et al. (2024) potential over the McMillan (2017) one. We therefore conclude that our conclusions are not significantly affected by the assumption that the potential is axisymmetric.

Separate from the adopted potential, a factor that might introduce additional angular momentum is scattering from individual stars. We assume implicitly in this work that this is negligible, but especially for stars that experience multiple pericentre passages through the dense GC region, scattering might become important. Since we only considered stars with apocenters outside the GC, we effectively limited the number of orbits for these stars. Indeed, we find that for stars with an apocenter greater than 1 kpc, the number of orbits is at most a few tens in our simula-

tions. We therefore assume that scattering by individual stars is not important.

7. Summary and conclusion

In this work, we searched for the population of GC ejecta that we expect has accumulated in the stellar halo over billions of years by the Hills mechanism and by massive black hole binary ejections. To this purpose, we used the newly released *DESI* DR1 in combination with simulations to predict the angular momentum distribution of stars ejected from the GC. We find that the radial distribution of GC ejecta between 1 and 100 kpc from the GC can be described by a single power law with $\rho \propto r^{-3.41 \pm 0.01}$. Gravitational focussing by the disc means that many stars ejected from the GC will end up in the stellar disc, making identification more challenging due to the large number of disc stars. We build a mixture model to describe the L_z distribution around $L_z = 0$ as a function of metallicity and fit this to the *DESI* data. We find that on a statistical level there is no overdensity at high metallicity of stars on low L_z orbits, as would be expected for GC ejecta. Based on this null-detection, we put a ejection model-independent upper limit on the ejection rate of stars from the GC of $\sim 2.8 \times 10^{-3} \text{ yr}^{-1}$. We also place a 95% upper limit on the number of GC ejecta at $|b| > 40 \text{ deg}$ and $16 < r < 19$ of 4.3×10^2 stars.

The analysis presented here can be repeated for other large spectroscopic surveys, for instance using the *Gaia* DR3 radial velocity subsample (Gaia Collaboration et al. 2023), *LAMOST* (Cui et al. 2012), or *APOGEE* (Majewski et al. 2017). Furthermore, the upcoming *Gaia* DR4 and *DESI* DR2 will significantly increase the number of sources on which this analysis can be applied. *DESI* DR2 for instance is expected to contain about three

times as many stars compared to DR1 (Koposov et al. 2025). Our method would be enhanced by considering additional tracers, such as elemental abundances, which would add weight to any claimed GC ejecta discoveries (see e.g. Hattori et al. 2025).

Our results can be used to constrain ejection mechanisms; a particularly interesting application is constraining the merger history of Sgr A* (Evans et al. in prep). Gravitational slingshots of single stars by a massive binary black hole eject stars with properties similar to the Hills mechanism (Yu & Tremaine 2003). Evans et al. (2023) already use this in combination with the lack of uncontroversial HVs in *Gaia* DR3 to constrain that mergers of Sgr A* with a possible companion of $> 500 M_{\odot}$ cannot have happened less than 10 Myr ago. Expanding on this, we expect that our non-detection of a population of bound ejecta constrains the merger history of Sgr A* on a timescale of billions of years, something we know very little about.

Acknowledgements. The authors thank Koen Kuijken, Manuel Cavieres Carrera, Adrian Price-Whelan, Carrie Filion, and Danny Horta for useful discussions. EMR and ZP acknowledge support from the European Research Council (ERC) grant number: 101002511/project acronym: VEGA. P. SK acknowledges support from the Science & Technology Facilities Council (STFC) grant ST/Y001001/1. We acknowledge the Gaia Project Scientist Support Team and the Gaia Data Processing and Analysis Consortium (DPAC). This work has made use of data from the European Space Agency (ESA) mission *Gaia* (<https://www.cosmos.esa.int/gaia>), processed by the *Gaia* Data Processing and Analysis Consortium (DPAC, <https://www.cosmos.esa.int/web/gaia/dpac/consortium>). Funding for the DPAC has been provided by national institutions, in particular the institutions participating in the *Gaia* Multilateral Agreement. This research used data obtained with the Dark Energy Spectroscopic Instrument (DESI). DESI construction and operations is managed by the Lawrence Berkeley National Laboratory. This material is based upon work supported by the U.S. Department of Energy, Office of Science, Office of High-Energy Physics, under Contract No. DE-AC02-05CH11231, and by the National Energy Research Scientific Computing Center, a DOE Office of Science User Facility under the same contract. Additional support for DESI was provided by the U.S. National Science Foundation (NSF), Division of Astronomical Sciences under Contract No. AST-0950945 to the NSF's National Optical-Infrared Astronomy Research Laboratory; the Science and Technology Facilities Council of the United Kingdom; the Gordon and Betty Moore Foundation; the Heising-Simons Foundation; the French Alternative Energies and Atomic Energy Commission (CEA); the National Council of Humanities, Science and Technology of Mexico (CONAHCYT); the Ministry of Science and Innovation of Spain (MICINN), and by the DESI Member Institutions: www.desi.lbl.gov/collaborating-institutions. The DESI collaboration is honored to be permitted to conduct scientific research on L'oligam Du'ag (Kitt Peak), a mountain with particular significance to the Tohono O'odham Nation. Any opinions, findings, and conclusions or recommendations expressed in this material are those of the author(s) and do not necessarily reflect the views of the U.S. National Science Foundation, the U.S. Department of Energy, or any of the listed funding agencies. For the purpose of open access, the author has applied a Creative Commons Attribution (CC BY) licence to any Author Accepted Manuscript version arising from this submission. Software: NumPy (Harris et al. 2020), SciPy (Virtanen et al. 2020), Matplotlib (Hunter 2007), Astropy (Astropy Collaboration et al. 2013, 2018, 2022), isochrones (Morton 2015), Speedystar (Contigiani et al. 2019; Evans et al. 2022a), emcee (Foreman-Mackey et al. 2013), Agama (Vasiliev 2019b).

References

Amarante, J. A. S., Koposov, S. E., & Laporte, C. F. P. 2024, *A&A*, 690, A166
 Astropy Collaboration, Price-Whelan, A. M., Lim, P. L., et al. 2022, *apj*, 935, 167
 Astropy Collaboration, Price-Whelan, A. M., Sipőcz, B. M., et al. 2018, *AJ*, 156, 123
 Astropy Collaboration, Robitaille, T. P., Tollerud, E. J., et al. 2013, *A&A*, 558, A33
 Bell, E. F., Zucker, D. B., Belokurov, V., et al. 2008, *ApJ*, 680, 295
 Belokurov, V., Erkal, D., Evans, N. W., Koposov, S. E., & Deason, A. J. 2018, *MNRAS*, 478, 611
 Belokurov, V., Sanders, J. L., Fattahi, A., et al. 2020, *MNRAS*, 494, 3880
 Bland-Hawthorn, J. & Gerhard, O. 2016, *ARA&A*, 54, 529
 Bromley, B. C., Kenyon, S. J., Geller, M. J., et al. 2006, *ApJ*, 653, 1194
 Bromley, B. C., Kenyon, S. J., Geller, M. J., & Brown, W. R. 2012, *ApJ*, 749, L42

Brown, W. R. 2015, *ARA&A*, 53, 15
 Brown, W. R., Geller, M. J., & Kenyon, S. J. 2014, *ApJ*, 787, 89
 Brown, W. R., Geller, M. J., Kenyon, S. J., & Kurtz, M. J. 2005, *ApJ*, 622, L33
 Brown, W. R., Geller, M. J., Kenyon, S. J., Kurtz, M. J., & Bromley, B. C. 2007, *ApJ*, 660, 311
 Brown, W. R., Lattanzi, M. G., Kenyon, S. J., & Geller, M. J. 2018, *ApJ*, 866, 39
 Choi, J., Dotter, A., Conroy, C., et al. 2016, *ApJ*, 823, 102
 Contigiani, O., Rossi, E. M., & Marchetti, T. 2019, *MNRAS*, 487, 4025
 Cooper, A. P., Koposov, S. E., Allende Prieto, C., et al. 2023, *ApJ*, 947, 37
 Cui, X.-Q., Zhao, Y.-H., Chu, Y.-Q., et al. 2012, *Research in Astronomy and Astrophysics*, 12, 1197
 Deason, A. J. & Belokurov, V. 2024, *New A Rev.*, 99, 101706
 DESI Collaboration, Abdul-Karim, M., Adame, A. G., et al. 2025, arXiv e-prints, arXiv:2503.14745
 DESI Collaboration, Aghamousa, A., Aguilar, J., et al. 2016, arXiv e-prints, arXiv:1611.00036
 Do, T., Kerzendorf, W., Winsor, N., et al. 2015, *ApJ*, 809, 143
 Dotter, A. 2016, *ApJS*, 222, 8
 Evans, F. A., Marchetti, T., & Rossi, E. M. 2022a, *MNRAS*, 512, 2350
 Evans, F. A., Marchetti, T., & Rossi, E. M. 2022b, *MNRAS*, 517, 3469
 Evans, F. A., Rasskazov, A., Rempelzwaal, A., et al. 2023, *MNRAS*, 525, 561
 Feldmeier-Krause, A., Veršič, T., van de Ven, G., Gallego-Cano, E., & Neumayer, N. 2025, arXiv e-prints, arXiv:2506.06014
 Feldmeier-Krause, A., Zhu, L., Neumayer, N., et al. 2017, *MNRAS*, 466, 4040
 Feuillet, D. K., Sahlholdt, C. L., Feltzing, S., & Casagrande, L. 2021, *MNRAS*, 508, 1489
 Foreman-Mackey, D., Hogg, D. W., Lang, D., & Goodman, J. 2013, *PASP*, 125, 306
 Gaia Collaboration, Prusti, T., de Bruijne, J. H. J., et al. 2016, *A&A*, 595, A1
 Gaia Collaboration, Vallenari, A., Brown, A. G. A., et al. 2023, *A&A*, 674, A1
 Gallo, A., Ostorero, L., Chakrabarty, S. S., Ebagezio, S., & Diaferio, A. 2022, *A&A*, 663, A72
 Harris, C. R., Millman, K. J., van der Walt, S. J., et al. 2020, *Nature*, 585, 357
 Hasselquist, S., Hayes, C. R., Lian, J., et al. 2021, *The Astrophysical Journal*, 923, 172
 Hattori, K., Taniguchi, D., Tsujimoto, T., et al. 2025, arXiv e-prints, arXiv:2502.20266
 Haywood, M., Di Matteo, P., Lehnert, M. D., et al. 2018, *ApJ*, 863, 113
 Helmi, A., Babusiaux, C., Koppelman, H. H., et al. 2018, *Nature*, 563, 85
 Hills, J. G. 1988, *Nature*, 331, 687
 Horta, D., Schiavon, R. P., Mackereth, J. T., et al. 2023, *MNRAS*, 520, 5671
 Hunt, J. A. S. & Vasiliev, E. 2025, *New A Rev.*, 100, 101721
 Hunter, G. H., Sormani, M. C., Beckmann, J. P., et al. 2024, *A&A*, 692, A216
 Hunter, J. D. 2007, *Computing in Science & Engineering*, 9, 90
 Kenyon, S. J., Bromley, B. C., Brown, W. R., & Geller, M. J. 2018, *ApJ*, 864, 130
 Kobayashi, S., Hainick, Y., Sari, R., & Rossi, E. M. 2012, *The Astrophysical Journal*, 748, 105
 Koposov, S. E. 2019, RVSpecFit: Radial velocity and stellar atmospheric parameter fitting, *Astrophysics Source Code Library*, record ascl:1907.013
 Koposov, S. E., Allende Prieto, C., Cooper, A. P., et al. 2024, *MNRAS*, 533, 1012
 Koposov, S. E., Boubert, D., Li, T. S., et al. 2020, *MNRAS*, 491, 2465
 Koposov, S. E., Li, T. S., Allende Prieto, C., et al. 2025, arXiv e-prints, arXiv:2505.14787
 Li, S., Wang, W., Koposov, S. E., et al. 2025, arXiv e-prints, arXiv:2503.02291
 Majewski, S. R., Schiavon, R. P., Frinchaboy, P. M., et al. 2017, *AJ*, 154, 94
 Marchetti, T., Evans, F. A., & Rossi, E. M. 2022, *MNRAS*, 515, 767
 McMillan, P. J. 2017, *MNRAS*, 465, 76
 Morton, T. D. 2015, isochrones: Stellar model grid package, *Astrophysics Source Code Library*, record ascl:1503.010
 Myeong, G. C., Vasiliev, E., Iorio, G., Evans, N. W., & Belokurov, V. 2019, *MNRAS*, 488, 1235
 Rix, H.-W. & Bovy, J. 2013, *A&A Rev.*, 21, 61
 Rossi, E. M., Kobayashi, S., & Sari, R. 2014, *The Astrophysical Journal*, 795, 125
 Sari, R., Kobayashi, S., & Rossi, E. M. 2009, *The Astrophysical Journal*, 708, 605
 Schödel, R., Nogueras-Lara, F., Gallego-Cano, E., et al. 2020, *A&A*, 641, A102
 Schultheis, M., Rich, R. M., Origlia, L., et al. 2019, *A&A*, 627, A152
 Vasiliev, E. 2019a, *MNRAS*, 482, 1525
 Vasiliev, E. 2019b, *MNRAS*, 482, 1525
 Verberne, S., Rossi, E. M., Koposov, S. E., et al. 2024, *MNRAS*, 533, 2747
 Verberne, S., Rossi, E. M., Koposov, S. E., et al. 2025, *A&A*, 696, A218
 Virtanen, P., Gommers, R., Oliphant, T. E., et al. 2020, *Nature Methods*, 17, 261
 Xue, X.-X., Rix, H.-W., Ma, Z., et al. 2015, *ApJ*, 809, 144
 Yu, F., Li, T. S., Speagle, J. S., et al. 2024, *ApJ*, 975, 81
 Yu, Q. & Tremaine, S. 2003, *ApJ*, 599, 1129
 Zhang, F., Lu, Y., & Yu, Q. 2013, *ApJ*, 768, 153